European Review for Medical and Pharmacological Sciences 2015; 19: 4241-4248

Creation of experimental aneurysms at a surgically created arterial confluence

Y.-Z. JIANG[1], Q. LAN[2], Q.-H. WANG[3], S.-Z. WANG[4], H. LU[1], W.-J. WU[1]

[1]Department of Neurosurgery, Wuxi Third People's Hospital, Wuxi, People's Republic of China
[2]Department of Neurosurgery, Second Affiliated Hospital of Soochow University, Suzhou, People's Republic of China
[3]Department of Neurosurgery, Ruijin Hospital of Jiaotong University, Shanghai, People's Republic of China
[4]Department of Mechanics and Engineering Science, Fudan University, Shanghai, China

Abstract. – OBJECTIVE: Complex vertebral confluence aneurysms remain clinically challenging despite the rapid technological advances in endovascular technology. Therefore, animal confluence aneurysm models are urgently needed for the preclinical development of related medical devices and training clinicians. This study aimed to establish canine confluence aneurysm model and evaluate hemodynamics in this model.

MATERIALS AND METHODS: According to the shape and regional blood flow of vertebrobasilar junction (VBJ) aneurysms, confluence aneurysm was introduced in 9 dogs by microsurgical technique. We partially anastomosed right common carotid artery (CCA) and left CCA (end to side anastomosis) to create inverted Y-junction of arteries and, then, sutured a harvested segment of external jugular vein to the notch of anastomosis to simulate confluence aneurysm. These animals were examined by 3D digital subtraction angiography (DSA) 4 weeks after surgery. Geometry parameters of the aneurysm, surrounding vasculature and specific double inlet profiles were analyzed by simulating computational fluid dynamics (CFD) in these animals.

RESULTS: Aneurysms were successfully established in all animals, including 8 complete and 1 partially thrombosed aneurysms. No neurological defects or death were observed. Geometric and hemodynamic parameters in these surgically introduced confluence aneurysm animals are similar to those reported for human VBJ aneurysms.

CONCLUSIONS: This study documents a protocol to successfully establish confluence aneurysm models in dogs. This model may be useful in preclinical studies targeting various complex vertebral confluence aneurysms.

Key Words:
Experimental aneurysm, Animal model, Arterial confluence, Dog.

Introduction

Endovascular coil embolization has recently become an effective method in the treatment of intracranial aneurysms. However, recanalization and life-threatening rerupture remain the major clinical obstacles in endovascular treatment, particularly in complex vertebral confluence aneurysms with wide-necked, larger or giant aneurysms[1-6]. Thus, the vertebral intracranial confluence aneurysms are often clinically challenging[6,7].

Animal models of confluence aneurysm are urgently needed for studying the hemodynamic properties, testing the long-term stability of new endovascular devices, and training surgeons in the highly challenging embolization techniques[8]. Unfortunately, most existing animal models for cerebral aneurysms are inadequate for these purposes. The descriptions of construction techniques for the confluence aneurysms are rarely reported. In this study, we established a new canine model of confluence aneurysm created by using a vein pouch at the arterial confluence of an end-to-side anastomosis at the carotid arteries, and demonstrated the possibility and feasibility of creating confluence aneurysms in canine.

Materials and Methods

Anesthesia and Intraoperative Monitoring

Nine mongrel dogs (both sexes), weighing 12.5-18 kg, were maintained on standard laboratory diet. After an overnight fast, the animals were anesthetized with an intraperitoneal injection of 4% pentobarbital 1 ml/kg with 22-gauge needles. All surgical procedures were performed

Corresponding Author: Qihong Wang, MD; e-mail: qihongwa@163.com

under sterile conditions using microsurgical techniques. After application of oropharynx breather, general anesthesia was maintained with additional doses of pentobarbital as required. Humidified oxygen was provided via the oropharynx breather tract to the animals, who could breathe spontaneously. The blood pressure, heart rate and temperature were monitored continuously during the operation. The study was performed according to the guidelines of the Committee on Ethics in Animal Experiments, Jiaotong University, Shanghai, China. Institutional approval for the animal study was obtained as required.

Aneurysm Construction

The animals were fixed in a supine position on the operating table, and their anterior necks were prepared and draped under sterile condition. A 10-cm midline incision between the larynx and sternum was made along the anterior neck. The right external jugular vein was isolated, and a 3.5-cm segment was ligated and resected between the ligatures. It was stored in heparinized saline at room temperature until needed for vein pouch creation. The pretracheal fascia was divided in the midline to expose both common carotid arteries (CCAs). The distal end of the left CCA was ligated while the proximal end was temporarily clamped. Then, the proximal segment of the divided left CCA was swung to the right in front of the trachea (Figure 1A). After vascular clamps were placed on the right CCA both proximally and distally, a partial end-to-side anastomosis of the left CCA to the proximal arteriotomy of the right CCA was created by interrupted monofilament 8-0 Nylon sutures. The adventitia must be meticulously removed from the edges of the vein graft and from the artery at the site chosen for the aneurysm. One corner of the proximal end of the left CCA was incised at a variable angle to create the desired size of the aneurysmal neck. An aneurysm sac was created from the resected vein and surgically attached to the notch formed by the anastomosis of both CCAs. Then, the clamp at the distal vein segment was opened briefly to remove captured thrombi. Finally, the dome of the aneurysm was ligated with a 6-0 suture to create the confluence aneurysm (Figure 1B-C) and closed the skin with a running suture. Aspirin therapy (75 mg daily) was continued for 4 weeks after surgery.

Angiographic Follow-Up

Under general anesthesia, transfemoral angiography (10) was performed at 4 weeks after surgery. Heparin (100 U/kg) was administered intravenously. A 4F catheter (Envoy; Cordis Endovascular, Freemont, CA, USA) was advanced into the brachiocephalic artery and left CCA, then standard intra-arterial digital subtraction angiography (IADSA) and 3D rotational angiography (3DRA) were performed. DSA angiograms were obtained in a plane that clearly depicted the aneurysm neck (Figure 2A).

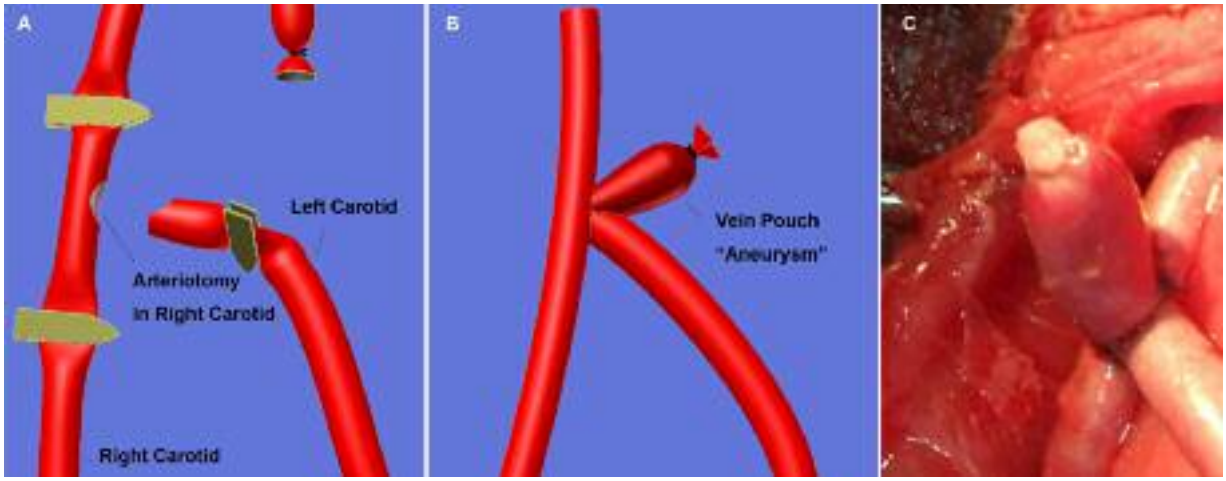

Figure 1. Illustrations depicting stages of grafting vein pouch to surgically constructed arterial confluence. ***A,*** Wedge is cut from medial corner of left common carotid artery and elliptical arteriotomy made in right common carotid artery. ***B,*** Partial end-to-side anastomosis of left common carotid artery to right common carotid artery is performed by using interrupted 7-0 nylon sutures; harvested vein segment is sutured to notch formed by anastomosis and open end of vein ligated with 6-0 silk suture to create aneurysm dome. ***C,*** Morphology of the venous pouch arterial bifurcation aneurysm after microsurgery.

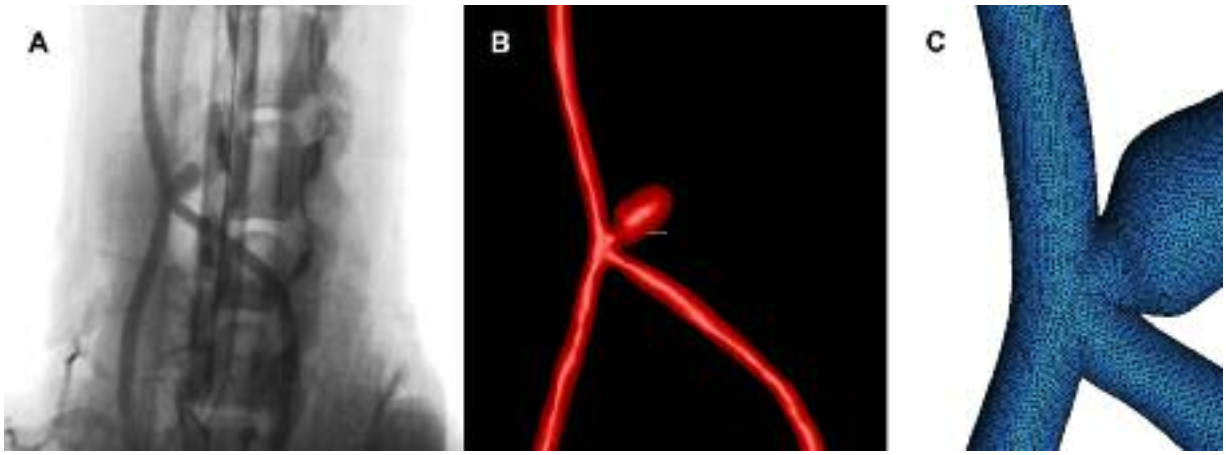

Figure 2. Construction of a canine vascular CFD model. ***A***, Original 3DRA image. ***B***, Smoothed and segmented vessel geometry. ***C***, Finite element grid.

Gross Morphometric Analysis

Aneurysm patency and dimensions, including neck diameter and aneurysm width and height, were measured from these DSA images in reference to external radiopaque sizing markers. An aneurysm that showed irregular dome filling of contrast material was regarded as a partially thrombosed aneurysm. An aneurysm that showed signs such as irregularity of the parent artery at the neck or no aneurysm filling was regarded as a completely thrombosed aneurysm. The aneurysm neck diameter was measured and the width of the aneurysm cavity was determined at its point of maximum measurement, while the height was measured from the aneurysm dome to the mid portion of a line connecting the proximal and distal portions of the aneurysm neck. The aneurysm aspect ratio (AR; height/neck width) was calculated[11].

Image Reconstruction and CFD Analysis

Canine confluence aneurysm models were constructed by using 3DRA data for the hemodynamic simulation. The rotational images were transferred to the angiography workstation (INTEGRIS 3D-RA, Philips Medical Systems, Cleveland OH, USA) and then a 3D reconstruction was performed. Using 3DMax software, the 3D VRML file was converted to the STL (Stereo Lithography format). Then the STL file was imported into Geomagic studio 9 (Geomagic Inc., Cary, NC, USA) software to repair, cut, and smooth (Figure 2B). The ICEM CFD 11.0 (Ansys, Inc., Canonsburg, PA, USA) was used to generate an advanced tetrahedral mesh inside the extracted surface (Figure 2C). After meshing, flow was, then, simulated in the resulting finite-volume model assuming the circulating fluid to be Newtonian and incompressible with attenuation = 1.0 g/cm^3 and viscosity μ = 0.04 Poise. Vessels were considered to be rigid tubes. The computational grid was imported into the commercial CFD package ANSYS CFX 11.0 (Ansys, Inc., Canonsburg, PA, USA) to simulate the blood flow. Visualizations of the distributions of hemodynamic forces (wall shear stress and pressure), intra-aneurysmal blood flow structure, and isovelocity surfaces were analyzed to determine zones of flow impaction, regions of elevated wall shear stress, and flow pattern.

Results

Surgical Procedures

Confluence aneurysms were successfully introduced into nine dogs with the above-described method. No peri- and postoperative mortality occurred. The whole procedure to construct an aneurysm takes approximately 120 min. None of the dogs showed neurological defects during follow-ups. All constructed aneurysms were angiographically patent during a 4-week follow-up period except for one, which was partially thrombosed.

Aneurysm Geometry

The dimensional geometric parameters of the nine cases for the canine model all fell within the range reported for human intracranial

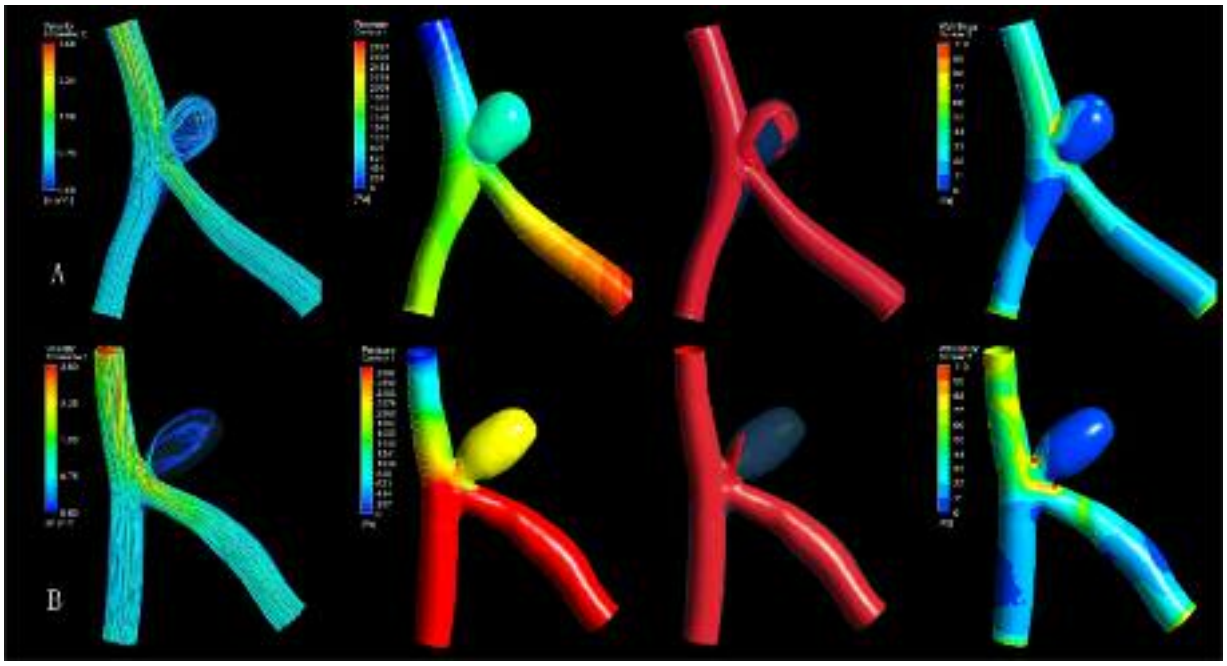

Figure 3. Hemodynamic results for representative low AR (A, AR <1.6) and high AR case (B, AR >1.6). From left to right, the visualization show flow streamlines, pressure distribution, isovelocity surfaces, and wall shear stress magnitude.

aneurysms[12-14], including aneurysm neck diameter, width, height, and AR (Table I). Neck diameters ranged from 2.52 to 7.25 mm (mean, 3.92 ± 1.68 mm), widths of aneurysm cavities ranged from 4.35 to 8.36 mm (mean, 5.62 ± 1.38 mm) and heights ranged from 6.20 to 16.56 mm (mean, 8.83 ± 2.61 mm). The average AR was 1.98 ± 0.53. The threshold value of 1.6 was used to distinguish low and high AR aneurysms[15,16] and 6 of 9 aneurysms had an AR greater than 1.6. Mean parent artery diameter was 4.6 ±1.9 mm.

Hemodynamic Properties of Aneurysms

Computational fluid dynamics simulation (CFD) was used to visualize the distribution of flow streamlines, pressure distribution, isovelocity surfaces, and wall shear stress magnitude. In all canine models, the flow streams from 2 CCAs confronted each other in the sagittal plane of the inverted Y-junction and then flow into the distal part of the right CCA. When the diameters of 2 CCAs were nearly equal, the fluid elements from 2 CCAs traveled almost parallel to the distal part of the right CCA without mixing with each other. In contrast to this, if the diameters of 2 CCAs differed significantly, the flow was disturbed as a result of swirling and secondary flows. The fluid entered the sac from the distal side and exited from the proximal side. The left column in figure 3 shows two typical intra-aneurysmal flow patterns. Type A (low AR) displayed an inflow jet with a single circulation inside the aneurysm sac. Type B (high AR) displayed an inflow jet with a primary (larger) circulation and a secondary cir-

Table I. Comparison of geometric features in canine aneurysms (N=9) and human aneurysms.

Geometric Features	Canine aneurysms		Human aneurysms[12-14]	
	Mean	Range	Mean	Range
Neck diameter (mm)	3.92 ± 1.68	2.52 - 7.25	Ruptured 3.79 ± 1.58; unruptured 4.25 ± 1.38	1.1–12.9
Width (mm)	5.62 ± 1.38	4.35 - 8.36	Ruptured 4.87 ± 1.86; unruptured 4.81 ± 1.37	1–11.4
Height (mm)	8.83 ± 2.61	6.20 - 16.56	Ruptured 6.55 ± 3.80; unruptured 5.13 ± 1.54	1.5–22.6
Aspect ratio (height/neck)	1.98± 0.53	0.72 – 3.50	Ruptured 1.85 ± 0.79; unruptured 1.27 ± 0.40	0.60–5.53

culation in the dome. The pressure was mostly uniform throughout the aneurysm sac, except for a small region around the point of flow impaction (second column). The inflow stream was visualized by using isovelocity surfaces. The velocity isosurface corresponding to v=25 cm/s is presented in the third column. These visualizations reveal a fairly concentrated inflow jet that impacts a relatively small region of the aneurysm wall. After impacting the wall, the inflow jet disperses into a wide umbrella-shaped structure along the aneurysm wall, filled with slower vortical structures toward the center of the aneurysm volume. Wall shear stress was markedly lower inside most of the sac and was elevated on the distal neck compared with the parent artery (right column).

Discussion

Animal aneurysm models have provided indispensable tool and knowledge for the hemodynamics and pathophysiology of intracranial aneurysms in humans. Numerous models have been used to test different coil systems and new surface materials for the endovascular obliteration of human cerebral aneurysms, such as lateral, bifurcation, and terminal aneurysm models[17]. Due to their complex wide necks and irregular shapes, and the incorporation of the branches of the basilar artery (BA)[6], intracranial vertebral confluence aneurysms are clinically challenging for both neurosurgeons and interventionists[6,7]. It is necessary to create suitable animal models to study their unique geometries and hemodynamics, and test new treatment methods. However, few confluence aneurysm models have been developed in the published studies. This could be due to the difficulty of performing surgical procedures, high morbidity and mortality. In this study, confluence aneurysms were successfully introduced into nine dogs, none of which died or showed neurological defects during follow-ups. The success of creating confluence aneurysms models depends on suitable animal, modified microsurgical techniques[9] and careful postoperative care.

Most previous reports of aneurysm models have relied on large animal models, including pigs, rabbits, and canine species[18-26]. The canine model used in our study offers advantages over other large animal models, including easy care and handling, reliable anesthesia, large vessels for simple surgical technique, the ease of performing multiple high-quality angiographic evaluations, the lack of spontaneous thrombosis or rupture, and excellent long-term survival[18,23,25,27-34]. The most common surgical construction technique for experimental aneurysms was developed by German and Black in 1954[20]. Since then, the canine vein pouch model has been widely used in the preclinical study of devices and training interventionists[35]. We have successfully produced a variety of aneurysm models using this technique[9]. In order to simulate the specific aneurysmal anatomical and hemodynamic characteristics, microsurgical techniques prove to be the most reliable to create a confluence aneurysm model. In our experimental model, a CCA-CCA crossover anastomosis was performed. After the distal end of the left CCA was ligated, a partial end-to-side anastomosis of the left CCA to the proximal arteriotomy of the right CCA was created by using interrupted sutures. The aneurysm sac was created from the resected vein and surgically attached to the notch formed by the anastomosis of both CCAs. Our confluence aneurysm model was designed to mimic closely human vertebral confluence aneurysms, which allows a partial transfer of the results to clinical circumstances. The unique characteristics of our experimental model are as follows: (1) despite of the sacrifice of one of the CCA, the confluence aneurysm can be created in a reproducible fashion without significant morbidity; (2) the arterial flow may be stronger in the confluence aneurysm model than that in the other models with two inflow vessels (the proximal part of left and right CCA) and one outflow vessel (the distal part of right CCA); (3) it recapitulates the hemodynamic properties and angiographic appearance of human vertebral confluence aneurysms; 4) the ability to vary the aneurysm size (neck diameter and aneurysm width and height); and 5) the caliber of the peripheral arteries allows the same animal to be treated multiple times with complex endovascular techniques.

In our work the geometric and hemodynamic parameters in confluence aneurysm models are similar to those reported in human IAs. From an anatomical point of view, the vertebrobasilar junction (VBJ) has a very unusual structure in that 2 large arteries (the left and right vertebral artery) join to form a larger-diameter artery (the basilar artery)[36]. The canine confluence aneurysm models share morphological features with those of VBJ aneurysms found in humans because they arise from a Y-shaped junction cre-

ated with both CCAs. When experimental studies for complex endovascular procedures and hemodynamic properties are designed by using canine confluence aneurysms, the geometric features can be predetermined to create a variety of aneurysm structures. The dimensional geometric parameters in these 9 confluence aneurysms all fell in the human range. The AR has been proposed as a useful index for predicting imminent aneurysm rupture[16,37]. Using microsurgical techniques, it was easy to create a good distribution of human AR. In our study, various complex confluence aneurysms can be constructed by changing the dimensional geometric parameters.

Digital simulations of the flow have recently conducted in aneurysm models and patients[38-45]. The computational fluid dynamics (CFD) study had two main limitations: 1) blood was approximated by a Newtonian model; 2) the vessel walls were considered rigid. However, these 2 factors are generally accepted as being of secondary importance compared with geometric and flow effects[40,41,45]. In our study, the CFD approach was used to determine the flow structure, isovelocity surfaces, wall shear stress, and pressure distribution within the confluence aneurysm model. The flow streams from 2 CCAs confronted each other as they flow into the distal part of the right CCA. The flow streams just coursed parallel to each other without mixing in the cases with nearly equal diameters of 2 CCAs. In contrast, the flow was disturbed as a result of swirling and secondary flows in the cases with very different diameters of 2 CCAs. These similar blood-flow properties of arterial confluence have been observed in the vertebrobasilar arterial trees in human[36]. Two typical intra-aneurysmal flow patterns and distributions of hemodynamic forces (pressure and wall shear stress) were demonstrated in this work. These characteristics were very similar to those of human vertebral confluence aneurysms[36,46]. The flow impingement zone of the canine models is always located at the distal neck, and a slow jet flow is observed at the distal wall. Cebral et al[46] found that unruptured aneurysms commonly exhibit simple stable flow patterns, large impingement regions, and large jet sizes, while ruptured aneurysms display disturbed flow patterns, small impingement regions, and narrow jets.

Even though our model can closely mimic the morphology and hemodynamics of human vertebral confluence aneurysms, the model still falls short in several aspects. The model requires sacrifice of one of the CAs, which increases risk of surgery. Fortunately, we have demonstrated that the carotid occlusion was well tolerated by all subjects. The lack of significant morbidity associated with carotid occlusion relates to the patency of the circle of Willis and robust leptomeningeal collateral present in dogs. Another potential criticism of our model is that long-term characteristics of these aneurysms were not assessed. However, canine aneurysms may infrequently undergo thrombosis and most aneurysms remained patent during a follow-up period of 7 months[35,47,48]. The patency period of our confluence aneurysms was also relatively long, with no evidence of spontaneous thrombosis up to 4 weeks after the procedure. It may be related to increased flow and aspirin therapy. Finally, the cohort was small which is limited by the substantial financial requirements, so a much larger sample size is necessary to reveal the same evidence.

Conclusions

We have developed a new canine model of confluence aneurysm with creation of a venous pouch between two CCA anastomoses, which is highly reproducible and technically less demanding. We suggest that this model may be useful in preclinical studies targeting various complex vertebral confluence aneurysms.

Funding

These work was supported by National Natural Science Foundation of China (81271304).

Conflict of Interest

The Authors declare that they have no conflict of interests.

References

1) Vinuela F, Duckwiler G, Mawad M. Guglielmi detachable coil embolization of acute intracranial aneurysm: perioperative anatomical and clinical outcome in 403 patients. J Neurosurg 1997; 86: 475-482.

2) Murayama Y, Nien YL, Duckwiler G, Gobin YP, Jahan R, Frazee J, Martin N, Viñuela F. Guglielmi detachable coil embolization of cerebral aneurysms: 11 years' experience. J Neurosurg 2003; 98: 959-966.

3) Brilstra EH, Rinkel GJ, van der Graaf Y, van Rooij WJ, Algra A. Treatment of intracranial aneurysms by embolization with coils: a systematic review. Stroke 1999; 30: 470-476.

4) Raymond J, Guilbert F, Weill A, Georganos SA, Juravsky L, Lambert A, Lamoureux J, Chagnon M, Roy D. Long-term angiographic recurrences after selective endovascular treatment of aneurysms with detachable coils. Stroke 2003; 34: 1398-1403.

5) Malisch TW, Guglielmi G, Vinuela F, Duckwiler G, Gobin YP, Martin NA, Frazee JG. Intracranial aneurysms treated with the Guglielmi detachable coil: midterm clinical results in a consecutive series of 100 patients. J Neurosurg 1997; 87: 176-183.

6) Horowitz MB, Levy EI, Koebbe CJ, Jungreis CC. Transluminal stent-assisted coil embolization of a vertebral confluence aneurysm: technique report. Surg Neurol 2001; 55: 291-296.

7) Wenderoth JD, Khangure MS, Phatouros CC, ApSimon HT. Basilar trunk occlusion during endovascular treatment of giant and fusiform aneurysms of the basilar artery. AJNR Am J Neuroradiol 2003; 24: 1226-1229.

8) Marbacher S, Erhardt S, Schlappi JA, Coluccia D, Remonda L, Fandino J, Sherif C. Complex bilobular, bisaccular, and broad-neck microsurgical aneurysm formation in the rabbit bifurcation model for the study of upcoming endovascular techniques. AJNR Am J Neuroradiol 2011; 32: 772-777.

9) Wang QH, Ma LT, Zhou ZH, Zhang XJ, Zhang ZH, Zhang XY, Shu F. Construction of the canine saccular aneurysm model: Modification of surgical technique and methods. Chinese Journal of Experimental Surgery 2005; 9: 1107-1108.

10) Bavinzski G, Al-Schameri A, Killer M, Schwendenwein I, Gruber A, Saringer W, Losert U, Richling B. Experimental bifurcation aneurysm: a model for in vivo evaluation of endovascular techniques. Minim Invasive Neurosurg 1998; 41: 129-132.

11) Lall RR, Eddleman CS, Bendok BR, Batjer HH. Unruptured intracranial aneurysms and the assessment of rupture risk based on anatomical and morphological factors: sifting through the sands of data. Neurosurg Focus 2009; 26: E2.

12) Parlea L, Fahrig R, Holdsworth DW, Lownie SP. An analysis of the geometry of saccular intracranial aneurysms. AJNR Am J Neuroradiol 1999; 20: 1079-1089.

13) Raghavan ML, Ma B, Harbaugh RE. Quantified aneurysm shape and rupture risk. J Neurosurg 2005; 102: 355-362.

14) Zeng Z, Kallmes DF, Durka MJ, Ding Y, Lewis D, Kadirvel R, Robertson AM. Hemodynamics and anatomy of elastase-induced rabbit aneurysm models: similarity to human cerebral aneurysms? Am J Neuroradiol 2011; 32: 595-601.

15) Ujiie H, Tamano Y, Sasaki K, Hori T. Is the aspect ratio a reliable index for predicting the rupture of a saccular aneurysm? Neurosurgery 2001; 48: 495-502, 502-503.

16) Weir B, Amidei C, Kongable G, Findlay JM, Kassell NF, Kelly J, Dai L, Karrison TG. The aspect ratio (dome/neck) of ruptured and unruptured aneurysms. J Neurosurg 2003; 99: 447-451.

17) Spetzger U, Reul J, Weis J, Bertalanffy H, Thron A, Gilsbach JM. Microsurgically produced bifurcation aneurysms in a rabbit model for endovascular coil embolization. J Neurosurg 1996; 85: 488-495.

18) Graves VB, Ahuja A, Strother CM, Rappe AH. Canine model of terminal arterial aneurysm. AJNR Am J Neuroradiol 1993; 14: 801-803.

19) Dawson RC, Krisht AF, Barrow DL, Joseph GJ, Shengelaia GG, Bonner G. Treatment of experimental aneurysms using collagen-coated microcoils. Neurosurgery 1995; 36: 133-139, 139-140.

20) GERMAN WJ, BLACK SP. Experimental production of carotid aneurysms. N Engl J Med 1954; 250: 104-106.

21) Graves VB, Partington CR, Rufenacht DA, Rappe AH, Strother CM. Treatment of carotid artery aneurysms with platinum coils: an experimental study in dogs. AJNR Am J Neuroradiol 1990; 11: 249-252.

22) Guglielmi G, Ji C, Massoud TF, Kurata A, Lownie SP, Viñuela F, Robert J. Experimental saccular aneurysms. II. A new model in swine. Neuroradiology 1994; 36: 547-550.

23) Massoud TF, Guglielmi G, Ji C, Vinuela F, Duckwiler GR. Experimental saccular aneurysms. I. Review of surgically-constructed models and their laboratory applications. Neuroradiology 1994; 36: 537-546.

24) Dawson RR, Shengelaia GG, Krisht AF, Bonner GD. Histologic effects of collagen-filled interlocking detachable coils in the ablation of experimental aneurysms in swine. AJNR Am J Neuroradiol 1996; 17: 853-858.

25) Mawad ME, Mawad JK, Cartwright JJ, Gokaslan Z. Long-term histopathologic changes in canine aneurysms embolized with Guglielmi detachable coils. AJNR Am J Neuroradiol 1995; 16: 7-13.

26) Tenjin H, Fushiki S, Nakahara Y, Masaki H, Matsuo T, Johnson CM, Ueda S. Effect of Guglielmi detachable coils on experimental carotid artery aneurysms in primates. Stroke 1995; 26: 2075-2080.

27) Raymond J, Guilbert F, Metcalfe A, Gevry G, Salazkin I, Robledo O. Role of the endothelial lining in recurrences after coil embolization: prevention of recanalization by endothelial denudation. Stroke 2004; 35: 1471-1475.

28) Strother CM, Graves VB, Rappe A. Aneurysm hemodynamics: an experimental study. AJNR Am J Neuroradiol 1992; 13: 1089-1095.

29) Raymond J, Salazkin I, Georganos S, Guilbert F, Desfaits AC, Gevry G, Weill A, Roy D. Endovascular treatment of experimental wide neck aneurysms: comparison of results using coils or cyanoacrylate with the assistance of an aneurysm neck bridge device. AJNR Am J Neuroradiol 2002; 23: 1710-1716.

30) Shin YS, Niimi Y, Yoshino Y, Song JK, Silane M, Berenstein A. Creation of four experimental aneurysms with different hemodynamics in one dog. AJNR Am J Neuroradiol 2005; 26: 1764-1767.

31) Bouzeghrane F, Naggara O, Kallmes DF, Berenstein A, Raymond J. In vivo experimental intracranial aneurysm models: a systematic review. AJNR Am J Neuroradiol 2010; 31: 418-423.

32) Yapor W, Jafar J, Crowell RM. One-stage construction of giant experimental aneurysms in dogs. Surg Neurol 1991; 36: 426-430.

33) Graves VB, Strother CM, Rappe AH. Treatment of experimental canine carotid aneurysms with platinum coils. AJNR Am J Neuroradiol 1993; 14: 787-793.

34) Sorteberg A, Sorteberg W, Rappe A, Strother CM. Effect of Guglielmi detachable coils on intraaneurysmal flow: experimental study in canines. AJNR Am J Neuroradiol 2002; 23: 288-294.

35) Turk AS, Aagaard-Kienitz B, Niemann D, Consigny D, Rappe A, Grinde J, Strother CM. Natural history of the canine vein pouch aneurysm model. AJNR Am J Neuroradiol 2007; 28: 531-532.

36) Kobayashi N, Karino T. Flow patterns and velocity distributions in the human vertebrobasilar arterial system. Laboratory investigation. J Neurosurg 2010; 113: 810-819.

37) Hassan T, Timofeev EV, Saito T, Shimizu H, Ezura M, Matsumoto Y, Takayama K, Tominaga T, Takahashi A. A proposed parent vessel geometry-based categorization of saccular intracranial aneurysms: computational flow dynamics analysis of the risk factors for lesion rupture. J Neurosurg 2005; 103: 662-680.

38) Meng H, Wang Z, Kim M, Ecker RD, Hopkins LN. Saccular aneurysms on straight and curved vessels are subject to different hemodynamics: implications of intravascular stenting. AJNR Am J Neuroradiol 2006; 27: 1861-1865.

39) Metaxa E, Tremmel M, Natarajan SK, Xiang J, Paluch RA, Mandelbaum M, Siddiqui AH, Kolega J, Mocco J, Meng H. Characterization of critical hemodynamics contributing to aneurysmal remodeling at the basilar terminus in a rabbit model. Stroke 2010; 41: 1774-1782.

40) Castro MA, Putman CM, Cebral JR. Computational fluid dynamics modeling of intracranial aneurysms: effects of parent artery segmentation on intra-aneurysmal hemodynamics. AJNR Am J Neuroradiol 2006; 27: 1703-1709.

41) Cebral JR, Castro MA, Appanaboyina S, Putman CM, Millan D, Frangi AF. Efficient pipeline for image-based patient-specific analysis of cerebral aneurysm hemodynamics: technique and sensitivity. Ieee Trans Med Imaging 2005; 24: 457-467.

42) Hassan T, Ezura M, Timofeev EV, Tominaga T, Saito T, Takahashi A, Takayama K, Yoshimoto T. Computational simulation of therapeutic parent artery occlusion to treat giant vertebrobasilar aneurysm. AJNR Am J Neuroradiol 2004; 25: 63-68.

43) Jou LD, Wong G, Dispensa B, Lawton MT, Higashida RT, Young WL, Saloner D. Correlation between lumenal geometry changes and hemodynamics in fusiform intracranial aneurysms. AJNR Am J Neuroradiol 2005; 26: 2357-2363.

44) Mantha A, Karmonik C, Benndorf G, Strother C, Metcalfe R. Hemodynamics in a cerebral artery before and after the formation of an aneurysm. AJNR Am J Neuroradiol 2006; 27: 1113-1118.

45) Steinman DA, Milner JS, Norley CJ, Lownie SP, Holdsworth DW. Image-based computational simulation of flow dynamics in a giant intracranial aneurysm. AJNR Am J Neuroradiol 2003; 24: 559-566.

46) Cebral JR, Castro MA, Burgess JE, Pergolizzi RS, Sheridan MJ, Putman CM. Characterization of cerebral aneurysms for assessing risk of rupture by using patient-specific computational hemodynamics models. AJNR Am J Neuroradiol 2005; 26: 2550-2559.

47) Kallmes DF, Altes TA, Vincent DA, Cloft HJ, Do HM, Jensen ME. Experimental side-wall aneurysms: a natural history study. Neuroradiology 1999; 41: 338-341.

48) Tsumoto T, Song JK, Niimi Y, Berenstein A. Interval change in size of venous pouch canine bifurcation aneurysms over a 10-month period. AJNR Am J Neuroradiol 2008; 29: 1067-1070.